MICROBIOLOGY

The kinases HipA and HipA7 phosphorylate different substrate pools in *Escherichia coli* to promote multidrug tolerance

Maja Semanjski[1], Elsa Germain[2]*, Katrin Bratl[1], Andreas Kiessling[1], Kenn Gerdes[2†], Boris Macek[1†]

The bacterial serine-threonine protein kinase HipA promotes multidrug tolerance by phosphorylating the glutamate-tRNA ligase (GltX), leading to a halt in translation, inhibition of growth, and induction of a physiologically dormant state (persistence). The HipA variant HipA7 substantially increases persistence despite being less efficient at inhibiting cell growth. We postulated that this phenotypic difference was caused by differences in the substrates targeted by both kinases. We overproduced HipA and HipA7 in *Escherichia coli* and identified their endogenous substrates by SILAC-based quantitative phosphoproteomics. We confirmed that GltX was the main substrate of both kinase variants and likely the primary determinant of persistence. When HipA and HipA7 were moderately overproduced from plasmids, HipA7 targeted only GltX, but HipA phosphorylated several additional substrates involved in translation, transcription, and replication, such as ribosomal protein L11 (RplK) and the negative modulator of replication initiation, SeqA. HipA7 showed reduced kinase activity compared to HipA and targeted a substrate pool similar to that of HipA only when produced from a high–copy number plasmid. The kinase variants also differed in autophosphorylation, which was substantially reduced for HipA7. When produced endogenously from the chromosome, HipA showed no activity because of inhibition by the antitoxin HipB, whereas HipA7 phosphorylated GltX and phage shock protein PspA. Initial testing did not reveal a connection between HipA-induced phosphorylation of RplK and persistence or growth inhibition, suggesting that other HipA-specific substrates were likely responsible for growth inhibition. Our results contribute to the understanding of HipA7 action and present a resource for elucidating HipA-related persistence.

INTRODUCTION

Bacteria are able to survive prolonged antibiotic treatments not only by acquiring resistance through genetic mutations but also by the presence of phenotypically distinct, drug-tolerant subpopulations of genetically uniform cells (*1*). Persisters are defined as phenotypic variants of normal bacterial cells that become transiently tolerant to antibiotics by restraining their growth and entering a dormant-like state in a stochastic manner (*2*, *3*). In the persistent state, cells become tolerant to the lethal action of antibiotics that mostly target cellular processes required for growth. After antibiotic removal, persisters are able to resume their growth and produce the same phenotypically heterogeneous population containing mainly antibiotic-susceptible cells plus a small fraction of tolerant cells that may cause relapse of bacterial infection (*4*). The clinical relevance of persisters is supported by the isolation of bacteria with mutations in specific genes that increase persistence without increasing resistance, such as *Escherichia coli* and *Pseudomonas aeruginosa* from patients with urinary tract infections or cystic fibrosis, respectively (*5*–*7*). Elucidating the mechanisms underlying persister formation and resuscitation is obviously crucial to develop approaches for their eradication. However, because of low frequencies of persister cells—typically one in 10^4 to 10^6—it has been challenging to study this phenomenon (*8*).

Bacterial persistence is often associated with toxin-antitoxin (TA) modules that are composed of two genes: one encoding a protein that interferes with essential cellular processes (the toxin) and another encoding an RNA or a protein that inhibits toxin activity (the antitoxin) (*9*, *10*). The first gene linked to persistence was *E. coli hipA* (*high persister gene A*), identified by the isolation of the gain-of-function allele *hipA7* (*11*). This allele, found also in clinical isolates of uropathogenic *E. coli* (*5*), showed an increase in persistence of up to 1000-fold due to two amino acid substitutions (G22S and D291A) in the HipA protein (*8*, *12*). The *hipA* gene and the adjacent upstream *hipB* gene constitute a type II TA module. Ectopic production of the wild-type HipA even at low amounts causes growth inhibition that can be counteracted by its cognate antitoxin HipB, which interacts directly with HipA (*13*). HipA and HipB form a protein complex that represses the *hipBA* operon by binding to classical operators in the *hipBA* promoter region (*14*). HipA is a serine-threonine protein kinase that phosphorylates glutamate-tRNA (transfer RNA) ligase (GltX, also known as glutamyl-tRNA synthetase), causing a halt in translation and induction of the stringent response and persistence (*15*, *16*). HipA-mediated phosphorylation of the conserved residue Ser^{239} inhibits GltX aminoacylation activity (*15*), thus preventing it from transferring glutamate to $tRNA^{Glu}$. Consequently, uncharged $tRNA^{Glu}$ accumulates at the ribosomal A site and stimulates the ribosome-associated (p)ppGpp (guanosine tetra- and pentaphosphate) synthase RelA, with the resulting (p)ppGpp acting as an alarmone that triggers the stringent response, thereby inducing persistence (*17*). Ribosomal protein L11 (RplK) interacts with deacylated tRNA (*18*) and is required for RelA activation (*19*, *20*).

The HipA7 mutant kinase has been used as a model for studying persistence (*1*, *2*, *21*) because bacterial populations carrying the *hipA7* allele exhibit survivor frequency of up to 1% when treated with ampicillin

[1]Proteome Center Tuebingen, Interfaculty Institute for Cell Biology, University of Tuebingen, Auf der Morgenstelle 15, 72076 Tuebingen, Germany. [2]Centre for Bacterial Stress Response and Persistence, Department of Biology, University of Copenhagen, Ole Maaloesvej 5, DK-2200 Copenhagen, Denmark.
*Present address: Laboratoire de Chimie Bacterienne, CNRS, L'Institut de Microbiologie de la Méditerranée, 31 Chemin Joseph Aiguier, 13009 Marseille, France.
†Corresponding author. Email: boris.macek@uni-tuebingen.de (B.M.); kgerdes@bio.ku.dk (K.G.)

(*8*, *11*, *12*), which is 10 to 1000 times higher than wild-type populations. This increase in persistence was explained by the weakened interaction between two HipA7 molecules in a higher-order promoter complex with HipB (*5*, *21*). In this complex that represses the *hipBA* operon, active sites of the wild-type HipA are normally blocked, rendering HipA inactive. On the basis of structural data (*5*), it was suggested that the G22S substitution in HipA impairs HipA7 dimerization and releases HipA7 from the promoter complex, causing derepression of the promoter and accumulation of free HipA7, which then leads to greater persistence. Although this model explains the persister phenotype of *hipA7*, it still remains elusive why HipA7 is seemingly less toxic than HipA. Whereas ectopically produced HipA induces persistence and inhibits growth through inhibition of primarily protein and RNA synthesis, *hipA7* induction has only minor effects on cell growth and protein synthesis but, nevertheless, increases persistence similarly to induction of wild-type *hipA* (*13*). This led to the suggestion that persistence and growth inhibition by HipA could be two separate phenotypes caused by two distinct functions of HipA (*13*). Bacterial serine-threonine kinases phosphorylate multiple protein substrates (*22*, *23*); thus, we assumed that HipA is likely to have more than one protein target, especially because it affects multiple essential cellular functions (*24*). We also hypothesized that the two kinase variants may have different substrate pools that could explain the differences in their phenotypes.

Here, we used a stable isotope labeling by amino acids in cell culture (SILAC)–based quantitative phosphoproteomic workflow (*25*) to study HipA- and HipA7-induced growth inhibition and persistence. We found that HipA targeted multiple substrates in addition to GltX, with some of them being ribosomal proteins or regulators of DNA replication and transcription. Conversely, HipA7 exhibited kinase activity toward mainly one target, GltX, when it was mildly overproduced from a plasmid or from the chromosome. HipA7 only targeted additional substrates when it was highly overproduced from a plasmid. Our results indicate that the two variants of HipA have different activities and substrate pools that may contribute to their different persistence and growth phenotypes.

RESULTS

HipA phosphorylates multiple proteins in addition to GltX

Our first goal was to characterize the proteome and the phosphoproteome of the persistent state associated with HipA kinase activity. Given that HipA affects several main cellular processes, we assumed that this kinase likely acts on additional targets in addition to the well-described substrate GltX (*15*, *16*). Kinase-substrate relationships are usually determined by using deletion mutants (*26*); however, because HipA production is very low and HipA is kept inactive by interaction with HipB in wild-type cells (*27*), we chose to screen for substrates using an established model in which HipA is mildly ectopically produced in growing cells and causes growth inhibition and persistence (*15*).

To screen for endogenous phosphorylation targets of HipA, we induced the gene encoding the kinase from an arabinose-responsive promoter in a low–copy number plasmid in *E. coli* K-12 cultured with stable isotope–labeled derivatives of lysine (SILAC methodology) and performed phosphoproteomic analysis using liquid chromatography coupled to tandem mass spectrometry (LC-MS/MS; Fig. 1A and fig. S1A). The overproduction of HipA inhibited cell growth and led to an increase in persistence compared to the empty plasmid (fig. S1B), as previously reported (*15*). Conversely, overproduction of HipB from an isopropyl-β-D-thiogalactopyranoside (IPTG)–inducible *lac* operon promoter counteracted HipA-induced toxicity and growth inhibition and resuscitated the cells (Fig. 1A). Combining two triple-label SILAC experiments with a common time point collected just before *hipA* induction at an optical density at 600 nm (OD_{600nm}) of 0.4 (Fig. 1A) enabled us to follow the relative change in serine, threonine, and tyrosine phosphorylation for individual proteins over time during HipA-induced growth inhibition (Fig. 1B) and HipB-induced resuscitation (Fig. 1C). Proteomic analysis confirmed the overproduction of HipA and HipB, together with proteins encoded by arabinose- and IPTG-inducible genes (fig. S1, C and D). In addition, time series clustering analysis revealed one cluster of proteins that significantly decreased in abundance during growth inhibition and returned to baseline upon resuscitation (fig. S1E). This cluster included chemotaxis-related proteins that are involved in cell motility, such as flagellin, and the chemotaxis proteins CheA, CheY, CheW, Tsr, and Tar.

In total, we identified 380 phosphorylation sites on 230 unique proteins in two independent experiments that showed a good correlation (fig. S1, F and G). Phosphorylation of GltX on Ser^{239} was one of the phosphorylation events with the largest change (Fig. 1B), which confirmed the efficacy of this model for identifying kinase targets. In addition to GltX, multiple proteins showed an increase in phosphorylation (Fig. 1, B and D), revealing that HipA kinase likely acts on multiple substrates under these specific conditions. Several of these phosphoproteins are part of the translation machinery, such as ribosomal proteins S4, S7, S9, S10, L11, and L31, whereas some are involved in the regulation of replication (SeqA) or transcription (RcsB, Fis, and Hns; Fig. 1E). After triggering resuscitation by HipB, phosphorylated GltX decreased to its initial abundance, and other phosphorylated peptides also followed similar declining pattern, albeit with a slower response and to a lesser extent (Fig. 1D). After we identified a repertoire of potential HipA targets, we next tested whether they shared a specific kinase target motif. We did not identify any substantial sequence similarity around the detected phosphorylation sites, indicating that HipA does not specifically recognize a common linear sequence motif. We also detected a previously unknown phosphorylation site on HipA at Ser^{359}. To investigate whether this site is functionally important, we constructed mutants of HipA in which Ser^{359} or the previously described Ser^{150} inhibitory autophosphorylation site was replaced with alanine to prevent phosphorylation or aspartate to mimic phosphorylation and analyzed their phosphoproteomes (fig. S1, I and J) (*28*, *29*). Whereas both phosphoablative and phosphomimetic mutations at Ser^{150} impaired the activity of HipA, as observed previously (fig. S1I) (*29*), the same changes at Ser^{359} did not affect HipA activity (fig. S1J). We also detected additional phosphorylation sites on HipA (Ser^{158}) and on GltX (Ser^{246}) that were modified to a much lesser extent and represented by spectra of lower quality. These could possibly result from the weak target motif specificity often seen in bacterial kinases, but we did not further investigate these phosphorylation sites.

To determine whether the detected phosphoproteins were direct substrates of HipA, we performed in vitro kinase assays on purified HipA, GltX, and two candidate substrates, SeqA and RplK. Purified His_6-RplK or SeqA-His_6 was incubated with His_6-HipA kinase, and adenosine triphosphate (ATP) was then analyzed by high-resolution MS (Fig. 1F). Phosphorylation of RplK on Ser^{102} was detected only when purified His_6-RplK was incubated with His_6-HipA and ATP,

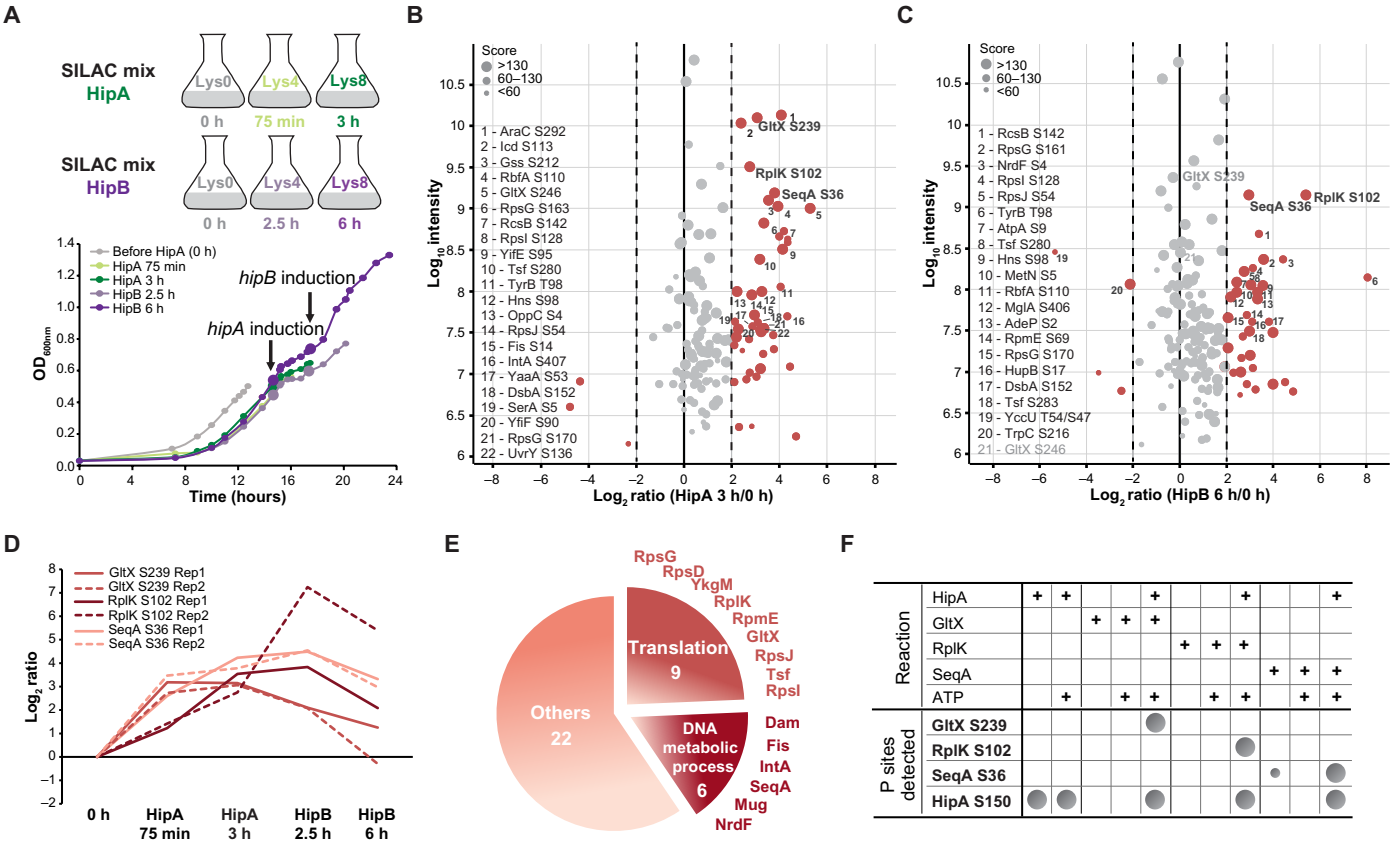

Fig. 1. Phosphoproteomic analysis of HipA-induced growth inhibition and HipB-induced resuscitation. (**A**) Growth curves of *E. coli* K-12 MG1655 carrying the pBAD33::*hipA* plasmid, in which *hipA* expression is under the control of an arabinose-inducible promoter, and the pNDM220::*hipB* plasmid, in which *hipB* is under the control of an IPTG-inducible promoter. Strains were grown in SILAC-labeled minimal medium containing stable isotope–labeled lysine derivatives: "light" lysine (Lys0), "medium-heavy" lysine (Lys4), or "heavy" lysine (Lys8), plus the appropriate antibiotics for retention of the plasmids. Expression of *hipA* was induced at OD_{600nm} of 0.4 with arabinose, and samples were collected before (Lys0) and 75 min (Lys4) and 3 hours (Lys8) after induction. At the 3-hour time point, *hipB* expression was induced with IPTG, and samples were collected 2.5 hours (Lys4) and 6 hours (Lys8) later. Growth curves are representative of two independent experiments. (**B** and **C**) Distribution of phosphorylation site SILAC ratios 3 hours after *hipA* expression (B) and 6 hours after *hipB* expression (C). The names of the phosphorylated proteins and the positions of the phosphorylation sites showing at least a fourfold increase in phosphorylation (red) are indicated. Distributions are representative of two independent experiments. (**D**) Phosphorylation site profiles of GltX, RplK, and SeqA over four time points during growth inhibition (HipA 75 min and HipA 3 hours) and resuscitation (HipB 2.5 hours and HipB 6 hours) in two independent experiments. (**E**) Gene ontology (GO) distribution of those phosphoproteins showing at least a fourfold increase in phosphorylation 3 hours after *hipA* expression enriched against the background of all identified phosphoproteins ($P < 0.01$). The number of enriched phosphoproteins is indicated below the category name, and the names of the proteins involved in translation and DNA metabolism are provided. The distribution is representative of two independent experiments. (**F**) In vitro kinase assay of His_6-HipA with His_6-GltX, His_6-RplK, and SeqA-His_6. After the phosphorylation reaction, the samples were protease-treated and analyzed by LC-MS/MS. Increased phosphorylation at the indicated sites represented as circles was detected in two independent experiments. The smaller circle depicted for SeqA indicates a two-order-of-magnitude lower intensity of phosphorylation site without His_6-HipA relative to the intensity measured in the presence of His_6-HipA.

suggesting that RplK is a substrate of HipA kinase. Phosphorylation of SeqA on Ser^{36} was detected already in purified SeqA-His_6 without addition of ATP, suggesting that SeqA is phosphorylated on Ser^{36} endogenously (Fig. 1F). However, the intensity of SeqA phosphorylation substantially increased in the presence of His_6-HipA, indicating that HipA phosphorylated SeqA in vitro. Together, our results show that overproduced HipA modifies multiple protein targets in addition to the canonical GltX.

RplK phosphorylation has no influence on RelA-dependent persistence

One of the particularly interesting HipA substrates identified in our phosphoproteomic analyses is RplK that is proposed to coordinate deacyl-tRNA for the activation of guanosine triphosphate (GTP) pyrophosphokinase RelA at the ribosome A site (*18*). Ribosome-bound RelA adopts an active conformation in the presence of a deacylated tRNA and synthesizes pppGpp from ATP and GTP and ppGpp from ATP and GDP (guanosine diphosphate) (*30*). To determine whether the phosphorylation of RplK influenced the activity of RelA, we engineered *rplK* phosphoablative and phosphomimetic mutations (*rplK S102A* and *rplK S102D*) into the endogenous genes on the chromosome and assessed cell viability on serine-methionine-glycine (SMG) M9 plates, which induce isoleucine starvation (*31*). Cell growth under this condition requires (p)ppGpp synthesis to induce isoleucine biosynthesis. As expected, the Δ*relA* mutant failed to grow on SMG plates due to its impaired ability to synthesize (p)ppGpp during amino acid starvation; however, *rplK* mutant strains were as viable as wild-type cells (fig. S1H). This implies that the phosphorylation

of RplK is not sufficient to influence RelA-dependent survival under amino acid starvation. However, this does not preclude a possible functional role of this phosphorylation event under different conditions or in combination with other HipA-induced phosphorylation events.

HipA7 has fewer in vivo substrates than HipA

To investigate the difference(s) in the kinase activities of toxic HipA and the less toxic variant HipA7, we induced the *hipA* or *hipA7* gene from the low–copy number plasmid and directly compared their phosphoproteomes (Fig. 2A). Despite apparently higher abundance of HipA7 in cells (fig. S2, A and B), only phosphorylation of GltX was common to both kinases, and we detected no additional targets for HipA7 (Fig. 2, B and C) in three independent experiments that showed a good reproducibility (fig. S2, C and D). This was in stark contrast to overproduction of HipA, which led to the phosphorylation of a wide range of proteins (Fig. 2C). We calculated the proportion of target proteins that were phosphorylated at the modification site (occupancy) using the relative abundances (SILAC ratios) of the modified peptide, its unmodified counterpart, and the total relative abundance of the protein (*32*). Because of the low abundance of the unphosphorylated form of the GltX peptide, we were able to determine the occupancy of the GltX phosphorylation site only for one experiment (fig. S2E). In the presence of HipA, 76% of GltX molecules were phosphorylated; this dropped to 48% in the presence of HipA7. The lower kinase activity of HipA7 toward GltX was additionally confirmed in vitro by autoradiography (fig. S2F). Together with fewer detected substrates, this implies that the two amino acid substitutions that distinguish HipA7 from HipA (G22S and D291A) reduce the activity of the kinase. Our phosphoproteomic data also revealed that 90% of HipA was autophosphorylated on Ser^{150}, and therefore inactive, whereas only 10% of HipA7 was autophosphorylated when overproduced (Fig. 2D). The autophosphorylation of HipA7 was also much lower than that of HipA when incubated with radioactive [γ-^{32}P]ATP in vitro (fig. S2G). We determined the phosphorylation site occupancy of the HipA substrates RplK and SeqA to be around 7% in the presence of HipA (Fig. 2, E and F).

Overproduction of HipA7, but not HipA, leads to increased abundance of multiple chaperones and proteases

Apart from the obvious differences in the substrate pools of the two forms of HipA, we also observed alterations in the proteome that depended on whether HipA or HipA7 was produced (fig. S2, A and B).

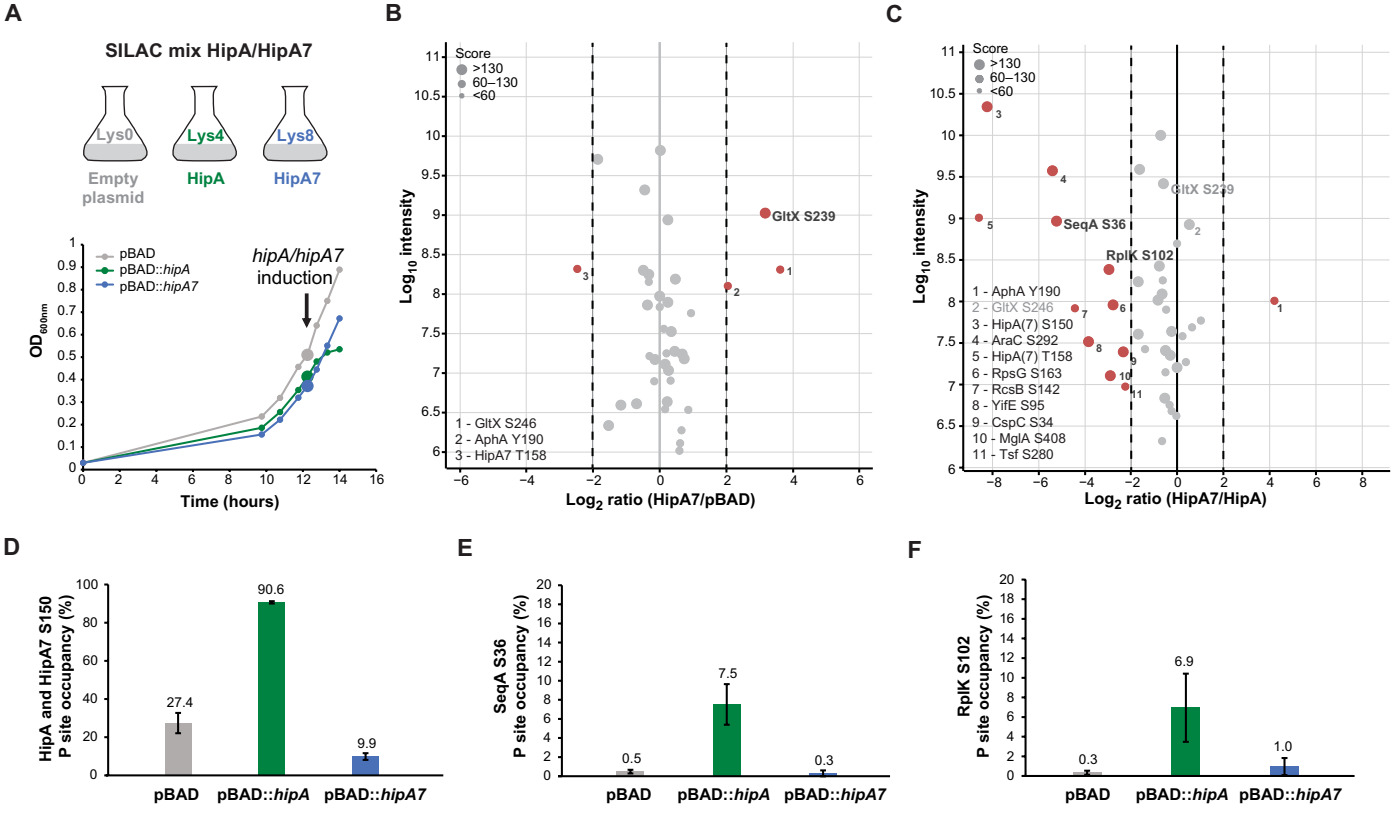

Fig. 2. Comparison of the phosphoproteomes of cells overproducing HipA or HipA7 in similar amounts. (**A**) Growth curves of MG1655 strains carrying either empty pBAD33 (pBAD), pBAD33::*hipA* (pBAD::*hipA*), or pBAD33::*hipA7* (pBAD::*hipA7*), in which *hipA* or *hipA7* expression is under the control of an arabinose-inducible promoter, and the pNDM220::*hipB* plasmid, in which *hipB* expression is under the control of an IPTG-inducible promoter. Strains were grown in SILAC-labeled minimal medium containing light lysine (Lys0), medium-heavy lysine (Lys4), or heavy lysine (Lys8) plus the appropriate antibiotics for retention of the plasmids. *hipA* or *hipA7* expression was induced at OD_{600nm} of 0.4 with arabinose, and samples were collected 95 min later. Expression of *hipB* was not induced in these experiments. Growth curves are representative of three independent experiments. (**B** and **C**) Distribution of phosphorylation site SILAC ratios 95 min after *hipA7* expression relative to the empty plasmid (B) and relative to *hipA* expression (C). The names of the phosphorylated proteins and the positions of the phosphorylation sites showing at least a fourfold change in phosphorylation (red) are indicated. Distributions are representative of three independent experiments. (**D**) Occupancy of the HipA and HipA7 Ser^{150} autophosphorylation site (P site) after *hipA* or *hipA7* expression determined by MaxQuant. (**E**) Occupancy of the SeqA Ser^{36} and (**F**) RplK Ser^{102} phosphorylation sites after *hipA* or *hipA7* expression calculated manually. Data in (D) to (F) are means ± SD from three independent experiments.

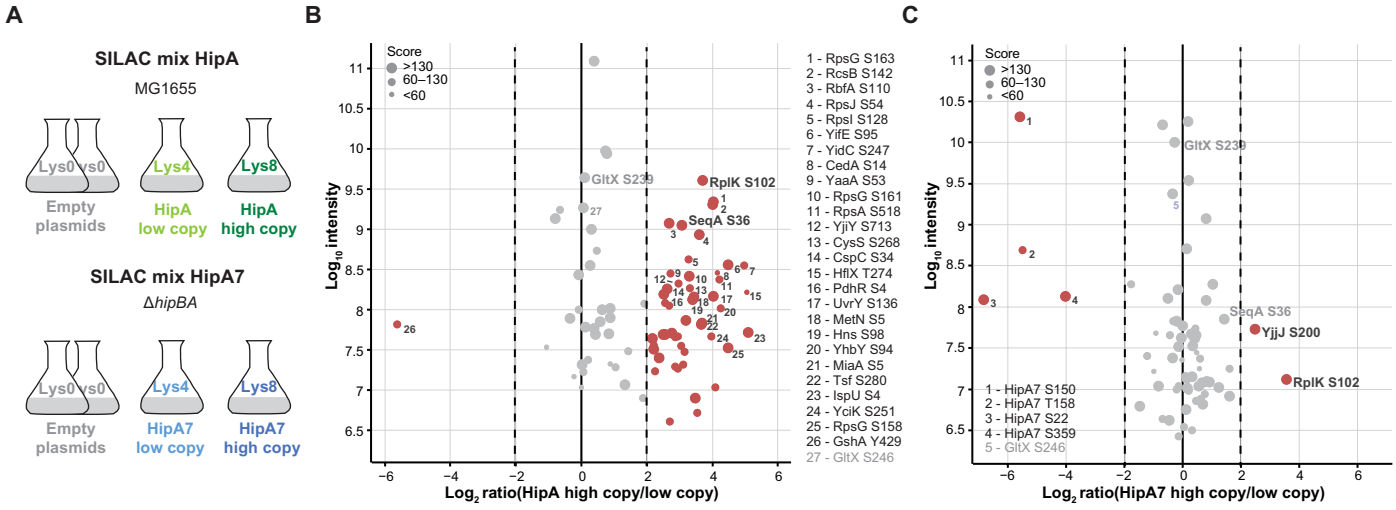

Fig. 3. Phosphoproteomic analysis of cells producing low or high amounts of HipA or HipA7. (**A**) Experimental setup of two SILAC experiments in which *hipA* or *hipA7* was induced from a low (pNDM220)– or a high (pMG25)–copy number plasmid, in which *hipA* or *hipA7* is under the control of an IPTG-inducible promoter in MG1655 *wt* strain (for *hipA* expression) or *hipBA* deletion mutant (Δ*hipBA*, for *hipA7* expression). Strains were grown in SILAC-labeled minimal medium containing light lysine (Lys0), medium-heavy lysine (Lys4), or heavy lysine (Lys8) plus ampicillin for retention of the plasmids. *hipA* or *hipA7* expression was induced at OD_{600nm} of 0.4 with IPTG, and samples were collected 95 min later. (**B** and **C**) Distribution of phosphorylation site SILAC ratios in cells, in which *hipA* (B) or *hipA7* (C) was induced from the high–copy number plasmid relative to expression from the low–copy number plasmid. The names of the phosphorylated proteins and the positions of the phosphorylation sites showing at least a fourfold change in phosphorylation (red) are indicated. Distributions are representative of two independent experiments.

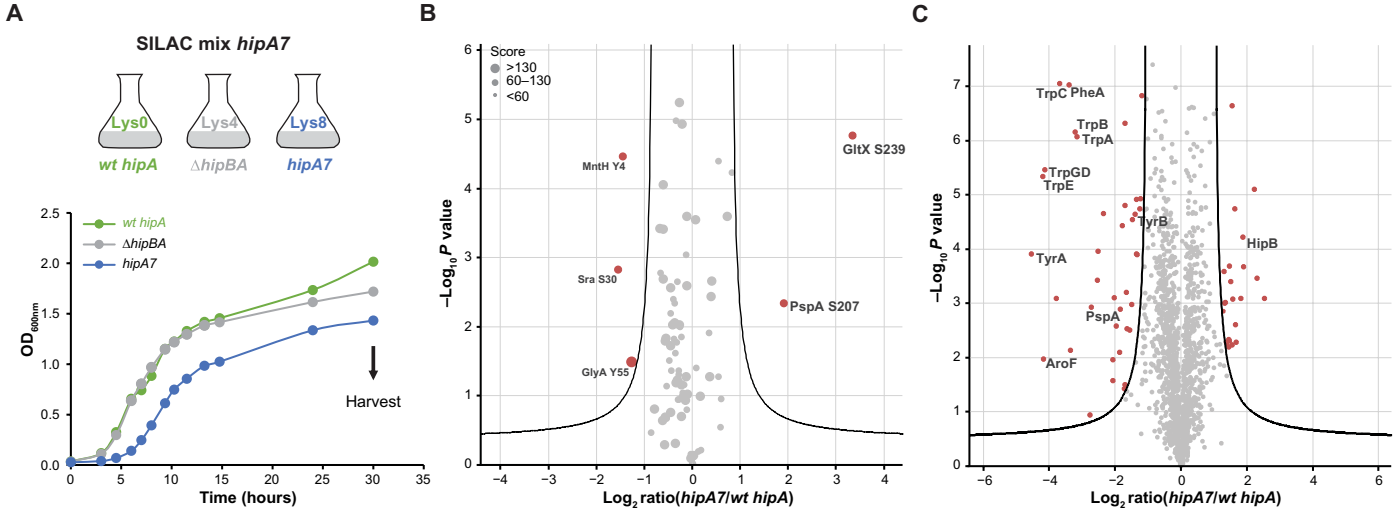

Fig. 4. Comparison of the phosphoproteomes of cells expressing *hipA7* or *hipA* from the endogenous *hipA* chromosomal locus. (**A**) Growth curves of three MG1655 strains: a strain carrying the wild-type *hipA* gene (*wt hipA*), a deletion mutant lacking both *hipB* and *hipA* (Δ*hipBA*), and a strain carrying the *hipA7* allele (*hipA7*) at the endogenous *hipA* locus. Strains were grown in SILAC-labeled minimal medium containing light lysine (Lys0), medium-heavy lysine (Lys4), or heavy lysine (Lys8), and samples were collected in the late stationary phase after 30 hours of growth. Growth curves are representative of three independent experiments. (**B**) Volcano plot of phosphorylation site SILAC ratios of the *hipA7* strain relative to the *wt hipA* strain from three independent experiments. The black curve indicates statistical significance with the *P* value of 0.01 and a minimal fold change of 1. The names of phosphorylated proteins and the positions of the phosphorylation sites that statistically significantly increased or decreased in phosphorylation (red) are indicated. (**C**) Volcano plot of protein SILAC ratios of the *hipA7* strain relative to the *wt hipA* strain from three independent experiments. The black curve indicates statistical significance with the *P* value of 0.001 and the minimal fold change of 1. Proteins statistically significantly increased or decreased in abundance are indicated in red. Names of HipB, PspA, and proteins of aromatic amino acid biosynthesis pathway are indicated in black text.

In particular, the components of the stress-induced multichaperone system (ClpB, DnaK, DnaJ, and GrpE) and other chaperones and chaperonins were significantly increased in abundance only in the presence of HipA7 but not in the presence of HipA (fig. S2B). GO term analysis of the proteins that increased in the presence of HipA7 revealed that protein folding was the most significantly enriched process (fig. S2H), and this group of proteins also included components of a proteasome-like degradation complex (HslU and HslV) and the Lon protease. Apart from components of the protein folding machinery, the abundance of the small heat shock proteins IbpA and IbpB that associate with aggregated proteins and protect them from proteolysis was significantly increased in the presence of HipA7 (fig. S2B).

This indicates that unfolding and refolding of proteins and protein aggregates, perhaps even of overproduced HipA7 itself, followed by their degradation, may be connected to the less toxic phenotype of HipA7. In addition, an autotransporter domain–containing protein that is involved in cell aggregation and biofilm formation, Antigen 43 (encoded by the gene *flu*), increased in abundance when HipA7 was overproduced (fig. S2B) (*33*).

Increasing the overproduction of HipA7 partially reproduces the molecular phenotype of mild HipA overproduction

To determine whether increasing the abundance of HipA7 could phenocopy mild overproduction of HipA, we increased the amount of HipA7 by expressing *hipA7* from a high–copy number plasmid rather than from a low–copy number plasmid. We cloned *hipA* and *hipA7* into both a low and a high–copy-number plasmid and performed phosphoproteomic analysis on cells carrying each plasmid using SILAC methodology (Fig. 3A and fig. S3, A and B). Compared to production from a low–copy number plasmid, production of HipA from a higher–copy number plasmid stimulated the phosphorylation of many more proteins in addition to previously identified targets such as RplK, SeqA, and RcsB (Fig. 3B and fig. S3C). GltX, on the other hand, was phosphorylated equally regardless of plasmid copy number. Compared to HipA, HipA7 showed a smaller repertoire of targets even when produced from the high–copy number plasmid (Fig. 3C and fig. S3D). However, under conditions of high HipA7 production, SeqA and RplK were phosphorylated, implying that HipA7 may partially reproduce the HipA phenotype when it is produced in higher amounts (Fig. 3C and fig. S3E). Phosphorylation of GltX, but not of SeqA and RplK, by HipA7 was confirmed in vitro (fig. S3F). Together, these results imply that HipA7 has weaker kinase activity than HipA. These phosphoproteomic analyses also identified several phosphorylation sites on HipA7 itself, one of which was Ser^{22}, a residue that is derived from the substitution of Gly^{22} in HipA (Fig. 3C).

Chromosomally encoded HipA7 phosphorylates GltX and phage shock protein PspA

We next investigated the difference between the HipA and HipA7 phosphoproteomes when the corresponding genes were induced from the chromosome, at the endogenous *hipA* locus, rather than from a plasmid. We compared the phosphoproteomes of stationary phase cultures of *E. coli* K-12 strain MG1655 in which *hipA* was replaced by the *hipA7* allele (*hipA7*) to deletion mutant lacking both *hipA* and *hipB* (Δ*hipBA*) and the wild-type strain having a wild-type copy of the *hipA* gene (*wt hipA*; Fig. 4A). In three independent experiments, we identified 665 phosphorylation sites on 374 proteins and quantified them with good reproducibility (fig. S4A). The results showed that chromosomally encoded HipA7 was able to phosphorylate GltX in the *hipA7* strain. GltX phosphorylation was 12-fold higher in the *hipA7* mutant than in the *wt hipA* strain (Fig. 4B). Accordingly, the *hipA7* strain grew slower and to a lower final OD_{600nm} at stationary phase (Fig. 4A), which is consistent with the greater phosphorylation of GltX (Fig. 4B). This apparently higher activity of HipA7 could be explained by an increase in the amount of the free, active kinase. Because of a weakened dimerization of HipA7 molecules, less HipA7 can interact with HipB, leaving more HipA7 available to target substrates. This causes increased *hipBA7* transcription due to a reduction in the repression of the *hipBA* operon by HipA-HipB heterodimers (*5*). From our proteomic data, we were only able to determine a total cellular abundance of HipA7 relative to HipA, and not the proportion of free HipA7 and HipA7 bound to HipB. Unexpectedly, the abundance of HipA7 was actually slightly lower than that of HipA (fig. S4D), raising the possibility that HipA7 is a less metabolically stable protein than HipA. In contrast, the abundance of HipB was fourfold higher in the *hipA7* than in the *wt hipA* strain, whereas the abundance of GltX did not change significantly (fig. S4D). Higher abundance of HipB in the *hipA7* strain could be explained by reduced *hipAB* promoter repression due to weakened interaction between the two HipA monomers in the promoter complex (*5*).

In addition to increased phosphorylation of GltX, phosphorylation of the phage shock protein PspA on Ser^{207} increased in the *hipA7* compared to the *wt hipA* strain (Fig. 4B). The abundance of the PspA protein was significantly lower (Fig. 4C), which raises the possibility that PspA protein stability may be influenced by phosphorylation. PspA is the negative regulator of a transcription factor PspF, which is associated with the expression of the phage shock protein (*psp*) operon in response to diverse stresses (*34*) and may play a role in persistence (*35*–*37*); however, we note that the abundances of other protein products of the *psp* operon were not changed in our data set (fig. S4F).

A direct comparison of the *wt hipA* and the Δ*hipBA* strains showed that GltX phosphorylation decreased significantly when *hipA* was deleted, which confirmed GltX phosphorylation by endogenous HipA (fig. S4B). However, under these conditions, the intensity of the GltX phosphopeptide was very low. This observation supports the need for using plasmid-encoded HipA to study its substrates. In addition to decreased phosphorylation of GltX, phosphorylation of the pantothenate synthetase (PanC) on Ser^{188}, a residue that is situated in the ATP-binding region of the enzyme, also decreased upon *hipA* deletion (*38*).

Although the phosphorylation status of proteins in the *hipA7* strain did not differ substantially from *wt hipA* cells, a direct comparison of their proteomes showed a major decrease in the abundance of proteins involved in the biosynthesis of aromatic amino acids (Fig. 4C and fig. S4, C and E). Those included the products of the entire tryptophan operon, aromatic amino acid aminotransferase (TyrB), chorismate mutase and prephenate dehydratases P-protein (PheA), and T-protein (TyrA). All of these proteins function downstream of chorismate in the shikimate pathway, where they convert chorismate into tyrosine, phenyalanine, and tryptophane through several distinct reactions. This observation provides a potential link between HipA7 activity and biosynthesis of aromatic amino acids.

E. coli phosphoproteome data sets are a resource for further investigation of phosphoregulation in bacteria

Finally, this study produced a substantial, high-quality phosphoproteome data set for *E. coli* K-12 containing a total of 2727 identified proteins and 1183 phosphorylation sites on 632 phosphoproteins (fig. S5A and data file S1). The proportion of serine, threonine, and tyrosine phosphorylation sites was comparable to previous studies (fig. S5B) (*39*, *40*). This data set enabled us to search for specific linear sequence motifs phosphorylated by bacterial serine-threonine kinases, which are still poorly investigated. Here, we report three common linear sequence motifs surrounding phosphorylation sites—two around phosphorylated serine residues and one around phosphorylated threonine residues (fig. S5C). All motifs contained a lysine residue, and in two of them, lysine was positioned immediately adjacent to the phosphorylation site, which is in agreement with a previous study (*39*). To determine which cellular functions are affected by

phosphorylation, we performed a functional enrichment of all identified phosphoproteins. We observed that serine, threonine, and tyrosine phosphorylation were spread across many essential cellular processes, such as translation, nucleotide metabolism, glycolysis and gluconeogenesis, the pentose phosphate pathway, aminoacyl-tRNA biosynthesis, and others (fig. S5D). Together, this data set will serve as a valuable resource for researchers interested in bacterial protein phosphorylation.

DISCUSSION

HipA is the only protein kinase among the type II TA modules in *E. coli* K-12 (*41*) that has been shown to strongly inhibit cellular growth and induce bacterial persistence by phosphorylating GltX (*15*). We hypothesized that HipA could phosphorylate additional protein targets, as shown for other bacterial kinases (*22*). Using high-resolution MS-based proteomics, we confirmed that endogenous GltX is phosphorylated when cell growth is inhibited by overproduced HipA, and we detected multiple additional HipA substrates implicated in replication and translation, such as SeqA and RplK. Although GltX has been established as a bona fide substrate of HipA, the phosphorylation of GltX on Ser^{239} by HipA had not previously been reported in vivo in a whole-cell lysate without overproduction of HipA and GltX, followed by GltX purification.

Our study identified several additional HipA targets that seem to be promising candidates for further analysis because of their role in essential cellular processes. For example, SeqA negatively regulates DNA replication by binding to newly replicated *oriC* regions, thereby preventing premature reinitiation of replication (*42*). The RcsB protein activates transcription of numerous genes involved in colonic acid capsule synthesis, biofilm formation, cell division, and synthesis of outer membrane proteins (*43*, *44*). In addition, 30*S* ribosomal protein S9 (RpsI) was phosphorylated at Ser^{128}, which is a part of a C-terminal tail that is important for the binding of specific tRNAs at the ribosomal P site (*45*).

Although we did not demonstrate the function of HipA-induced phosphorylation of RplK in the context of RelA-mediated persistence, we believe that the role of RplK in translation is more complex than initially thought. Because RplK is a part of the ribosomal stalk that helps the ribosome to interact with translation factors (*46*), it would be interesting to analyze the effects of phosphorylation mutants on translation fidelity and termination. Moreover, serine-threonine kinases phosphorylate their substrates less efficiently than do histidine kinases (*22*). This enables fine-tuning of the signaling system, suggesting that several proteins may need to be simultaneously phosphorylated to relay the signal that leads to growth inhibition and persistence. Therefore, to observe the effects of these phosphorylation events, a bacterial strain containing mutations in multiple HipA substrate phosphorylation sites should be constructed.

In contrast to HipA, which showed a large pool of targets when overproduced, its gain-of-function variant HipA7 exclusively phosphorylated GltX under the same expression conditions. This suggests that phosphorylation of GltX is the main molecular event required for induction of persistence by both HipA and HipA7, whereas phosphorylation of other protein targets likely leads to the toxic phenotype that is observed only for HipA overproduction. Although the amino acid substitutions in HipA7, G22S, and D291A were previously shown to weaken HipA7 homodimerization for formation of the $HipA_2$-$HipB_4$ promoter-binding complex and increase *hipBA7* transcription (*5*), it was not known whether these mutations alter the kinase activity of HipA. It had been suggested that the catalytic activity of HipA is not affected by these substitutions because the active site is located far from Gly^{22} and Asp^{291} (*29*). However, our in vivo phosphoproteomic analyses of cells overexpressing *hipA* and *hipA7* (Figs. 2 and 3) and in vitro phosphorylation experiments with purified HipA and HipA7 in the absence of HipB (fig. S2, F and G) demonstrated that HipA7 is a less active kinase than HipA. Therefore, the less toxic phenotype of HipA7 could also be explained by the lower activity of HipA7 toward GltX, leaving enough nonphosphorylated, active GltX available to sustain the cell growth. The two amino acid substitutions in HipA7 might also impair substrate binding or specificity, leading to the existence of a larger pool of substrates that are phosphorylated by HipA but not by HipA7. Together, this could explain the inability of HipA7 to elicit growth inhibition; however, this hypothesis needs to be further investigated. Our analysis of the phosphorylation site occupancy indicated that the vast majority (90%) of HipA was autophosphorylated upon induction from a plasmid (Fig. 2D), leaving only 10% of the kinase in its active form. Conversely, HipA7 showed much lower phosphorylation of Ser^{150}, which excludes the possibility that autophosphorylation is responsible for lower activity of HipA7.

Here, we present direct evidence that endogenous GltX is phosphorylated by chromosomally encoded HipA7 in the *hipA7* strain. Although HipA7 was less abundant than HipA (fig. S4D) and showed a weaker kinase activity in vitro (fig. S2, F and G), the increase in GltX phosphorylation that occurred when HipA7 was produced from the endogenous *hipA* locus could be explained by (i) a disrupted interaction between HipA7 and HipB that leads to a higher abundance of the free, active form of HipA7 or (ii) the reduced ability of HipA7 to inhibit its own kinase activity by autophosphorylation. This latter possibility would cause the entire pool of HipA7 to be weakly active. In contrast, HipA, which has a more potent kinase activity than HipA7, is inhibited by its interaction with HipB. With the exception of PspA and GltX, phosphorylation of other targets by chromosomally encoded HipA7 was not detected. However, higher amounts of HipA7 (produced from a high–copy number plasmid) stimulated the phosphorylation of another *E. coli* toxin YjjJ, the function of which is so far unknown but is likely to have a kinase activity (*47*). YjjJ was phosphorylated at Ser^{200} (or Ser^{201}), which is a conserved autophosphorylation site corresponding to Ser^{150} of HipA. Therefore, it would be interesting to determine the substrate(s) of YjjJ and investigate the link between YjjJ and HipA7.

In addition to information about phosphorylation, our data also provide an extensive resource of proteomic changes associated with HipA and HipA7. In particular, a connection between HipA7 and Antigen 43 was observed whether *hipA7* was ectopically induced from a plasmid or induced endogenously from the chromosome. Antigen 43 is a self-associating adhesin that stimulates biofilm formation and is produced by uropathogenic *E. coli* and promotes long-term persistence in urinary tract infections (*48*). It is tempting to speculate that the presence of HipA7 may trigger the production of Antigen 43, the presence of which in the outer membrane could cause the aggregation of *E. coli* cells and lead to the increase in drug tolerance.

MATERIALS AND METHODS

Bacterial strains and plasmids

E. coli strains and plasmids used in this study are listed in table S1. Because of its high toxicity, *hipA* was cloned into expression plasmids

together with a Shine-Dalgarno sequence in which the consensus sequence of the Shine-Dalgarno, the spacer between the Shine-Dalgarno and the start codon, or the start codon was changed to decrease the translation efficiency and the toxicity of HipA (*49*). In table S1, sd8 indicates a consensus sequence AAGGAA with a spacer of eight nucleotides to the ATG start codon. Oligonucleotides used are listed in table S2.

pNDM220::*hipA* and pNDM220::*hipA7*. The *hipA* gene was amplified from pEG5 and *hipA7* from pEG9 with primers OMS43 and OMS44. The polymerase chain reaction (PCR) products were digested with Eco RI and Bam HI and ligated with pNDM220 digested with the same enzymes. The resulting plasmids contain the *hipA* or *hipA7* gene with a mitigated Shine-Dalgarno (sd8ATG) sequence downstream of the P_{lac} promoter.

pMG25::*hipA* and pMG25::*hipA7*. The *hipA* gene was amplified from pEG5 and *hipA7* from pEG9 with primers OMS41 and OMS42. The PCR products were digested with Eco RI and Bam HI and ligated with pMG25 digested with the same enzymes. The resulting plasmids contain the *hipA* or *hipA7* gene with a mitigated Shine-Dalgarno (sd8ATG) sequence downstream of the P_{lac} promoter.

pBAD33::*6his hipA* and pBAD33::*6his hipA7*. The *hipA* gene was amplified from pEG5 and *hipA7* from pEG9 with primers OEG110 and OEG111. The PCR products were digested with Xba I and Sph I and ligated with pBAD33 digested with the same enzymes. The resulting plasmids contain the *hipA* or *hipA7* gene with a mitigated Shine-Dalgarno (sd8ATG) sequence downstream of the P_{BAD} promoter and the sequence that encodes six histidine residues at protein N terminus.

pBAD33::*hipA S150A*, pBAD33::*hipA S150D*, pBAD33::*hipA S359A*, and pBAD33::*hipA S359D*. Those mutants were amplified using a two-step PCR technique that consists of PCR amplification of each fragment upstream and downstream of the point mutation and then a third PCR mixing of both fragments to obtain *hipA* variant with the external primers OEG57 and OEG111. The *hipA* gene was amplified from pEG5 with primer pairs OEG57-OEG28 and OEG29-OEG111 to construct the S150A mutant, primer pairs OEG57-OEG242 and OEG241-OEG111 to construct the S150D mutant, primer pairs OEG57-OEG244 and OEG243-OEG111 to construct the S359A mutant, and primer pairs OEG57-OEG246 and OEG245-OEG111 to construct the S359D mutant. The final PCR products were digested with Xba I and Sph I and ligated with pBAD33 digested with the same enzymes. The resulting plasmids contain the *hipA* mutant gene with a mitigated Shine-Dalgarno (sd8ATG) sequence downstream of the P_{BAD} promoter.

pET28a::*gltX* and pET28a::*rplK*. The *gltX* and *rplK* genes were amplified from MG1655 *E. coli* strain with primer pairs OMS14-OMS15 and OMS3-OMS4, respectively. The PCR products were digested with Nde I and Xho I and ligated with pET28a digested with the same enzymes. The resulting plasmids contain the *gltX* or *rplK* gene, together with the sequence upstream of the *gltX* or *rplK* gene that, at protein N terminus, encodes for MGSS, six histidine residues, and SSGLVPRGSHM.

pET28a::*seqA*. The *seqA* gene was amplified from MG1655 with primers OMS26 and OMS27. The PCR product was digested with Nco I and Xho I and ligated with pET28a digested with the same enzymes. The resulting plasmid contains the *seqA* gene together with the sequence upstream of the *seqA* gene that encodes for the MA sequence at protein N terminus and the sequence downstream of the *seqA* gene that encodes for the LE sequence and six histidine residues at protein C terminus.

The MG1655 *rplK S102A* and *rplK S102D* strains were constructed by replacing a chromosomal *rplK* gene that encodes for RplK with the *rplK* gene that encodes for phosphoablative mutant RplK-S102A or phosphomimetic mutant RplK-S102D. To construct the mutants, two or three point mutations were introduced into the wild-type *rplK* gene (*gcg* codon for *rplK S102A* and *gat* for *rplK S102D* instead of *tcc* codon) at the position that encodes for Ser^{102}. Those mutants were amplified using a two-step PCR technique, as described above. The external primers used to obtain *rplK* variant were OMS20 and OMS21. *rplK S102A* was constructed using OMS20-OMS11 and OMS10-OMS21, and for *rplK S102D* variant, we used OMS20-OMS13 and OMS12-OMS21 (table S2). The gene constructs containing *nusG*, *rplK S102A*/*rplK S102D*, and *rplA* genes were cloned into the pKOV plasmid using Not I and Xba I restriction enzymes with primers OMS20 and OMS21, and allelic replacement was performed as previously described (*50*). The pKOV plasmid was a gift from G. Church (Addgene plasmid #25769). Colonies were screened for mutations using temperature switch PCR genotyping, as previously described (*51*) and confirmed by DNA sequencing.

Media and antibiotics

Cells were grown in LB (Roth) or in M9 minimal medium (50 mM Na_2HPO_4, 22 mM KH_2PO_4, 8.6 mM NaCl, 18.7 mM NH_4Cl, 1 mM $MgSO_4$, 0.1 mM $CaCal_2$, and 0.0001% thiamine) supplemented with either 0.5% glucose or 0.4% glycerol when using strains carrying pBAD33 plasmid constructs. Cultures were grown in batch at 37°C shaking at 200 rpm. When required, the medium was supplemented with chloramphenicol (25 μg/ml), ampicillin (25 to 50 μg/ml), or kanamycin (50 μg/ml). Plasmids carrying the P_{BAD} promoter were repressed in precultures by 0.4% D-(+)-glucose at OD_{600nm}. The expression of gene constructs on plasmids carrying the P_{BAD} promoter was induced with 0.2% L-(+)-arabinose at OD_{600nm} of around 0.4. The expression of gene constructs on plasmids carrying P_{lac} promoter was induced with 0.5 to 2 mM IPTG, 2 mM IPTG for pNDM220::*hipB* plasmid, and 1 mM IPTG for pNDM220 and pMG25 plasmid constructs with *hipA* and *hipA7*.

SILAC labeling

For quantitative (phospho)proteomic experiments, *E. coli* cells were differentially labeled using the following stable isotope–labeled lysine derivatives: 4,4,5,5-D_4 L-lysine (Lys4, medium-heavy lysine, K4, Cambridge Isotope Laboratories), $^{13}C_6{}^{15}N_2$ L-lysine (Lys8, heavy lysine, K8, Cambridge Isotope Laboratories), or L-lysine (Lys0, light lysine, K0, Sigma-Aldrich) (*52*). Both precultures and main cultures were grown in M9 minimal medium containing 0.0025% (w/v) Lys0, Lys4, or Lys8. The experimental design of all experiments is summarized in table S3.

Cell lysis and protein extraction

Cultures were harvested at specific stages by centrifugation at 4°C and stored at −80°C. The cell pellets were resuspended in a lysis buffer [SDS (40 mg/ml), 100 mM tris-HCl (pH 8.6), 10 mM EDTA, 5 mM glycerol-2-phosphate, 5 mM sodium fluoride, 1 mM sodium orthovanadate, and complete protease inhibitors (Roche)] and sonicated at least five times for 30 s at 40% amplitude. The cellular debris was pelleted by centrifugation at 13,000*g* for 30 min, and the crude protein extract was precipitated from the supernatant with methanol and chloroform. Protein pellet was resuspended in a denaturation buffer containing 6 M urea, 2 M thiourea, and 10 mM tris (pH 8.0). Protein concentration was measured using standard Bradford assay (Bio-Rad).

Protein digestion in solution

In each SILAC experiment, differently labeled protein extracts were mixed in equal amounts corrected by the ratios determined by measuring mixing checks (see below) to a total of 12 mg. Proteins were reduced using 1 mM dithiothreitol (DTT) for 1 hour and subsequently alkylated with 5.5 mM iodoacetamide for 1 hour. One-half of the protein mixture was diluted with four volumes of 62.5 mM tris (pH 8.0) and 12.5 mM $CaCl_2$ and digested with chymotrypsin (1:120, w/w) overnight at room temperature (RT). The other half was predigested with endoproteinase Lys-C (1:100, w/w) for 3 hours, then diluted with four volumes of 62.5 mM tris (pH 8.0), and supplemented with endoproteinase Lys-C (1:100, w/w) for overnight digestion at RT. The reaction was stopped by acidification with trifluoroacetic acid (TFA) to pH 2. An aliquot of 10 μg was purified by StageTips (see below), and 2 μg was used for direct proteome measurement with 230-min LC gradient. An additional aliquot of at least 100 μg intended for further proteome measurements was stored at −80°C.

Phosphopeptide enrichment

Digested peptides were desalted by the solid-phase extraction using Sep-Pak C18 Vac 100 mg column (Waters). Briefly, column was activated with methanol and equilibrated with solvent A* [2% (v/v) acetonitrile and 1% (v/v) formic acid]. After loading the sample, the column was washed with solvent A [0.1% (v/v) formic acid], and peptides were eluted with 1.8 ml of 80% (v/v) acetonitrile and 6% (v/v) TFA. Phosphopeptides were enriched by titanium dioxide (TiO_2) chromatography. Eluted peptides were incubated with TiO_2 spheres (5 μm, 300 Å, ZirChrom) in 1:10 peptide to bead ratio for 10 min for 5 to 10 consecutive rounds. TiO_2 spheres were washed twice with 80% (v/v) acetonitrile and 6% (v/v) TFA and loaded onto C8 (Empore) StageTips. The spheres were washed additionally with 80% (v/v) acetonitrile and 1% (v/v) TFA. Phosphopeptides were first eluted with 50 μl of 1.25% (v/v) ammonium hydroxide of pH 10.5 into 20 μl of 20% (v/v) TFA for 15 min at 1200 rpm. In the second elution step, phosphopeptides were eluted with 50 μl of 5% (v/v) ammonium hydroxide in 60% (v/v) acetonitrile (pH 10.5). Acetonitrile was evaporated from eluates by vacuum centrifugation, and samples were acidified to pH 2, if necessary, and purified by StageTips (see below).

High-pH reversed-phase peptide fractionation on commercial spin columns

To obtain a deeper coverage of proteome samples, peptides from one replicate of each experiment were additionally separated offline using a high-pH reversed-phase peptide fractionation kit (catalog no. 84868, Thermo Fisher Scientific) according to the manufacturer's instructions. Briefly, 50 μg of SILAC mixture was loaded onto the spin column, and peptides were eluted in the gradient of acetonitrile in nine fractions. The pH of 10 was maintained constant with 10 mM ammonium hydroxide instead of trimethylamine. Eluted fractions were concentrated by vacuum centrifugation and purified by StageTips (see below). Fractions were measured separately by LC-MS/MS using optimized LC gradients.

Offline high-pH reversed-phase peptide fractionation

Chymotrypsin-digested sample of one independent experiment of chromosomal *hipA7* (Rep1) was fractionated using an offline peptide fractionation at high pH to increase sequence coverage and detect unmodified GltX peptide. Peptides were loaded onto a reversed-phase XBridge BEH130 C18 3.5 μm 4.6 × 250 mm column installed in an UltiMate 3000 HPLC and detected by ultraviolet at λ = 214 nm at 25°C. The system was operated under basic conditions using buffer A (5 mM NH_4OH) and buffer B (5 mM NH_4OH in 90% acetonitrile) at pH 10. Peptides were eluted using an 80-min gradient at a flow rate of 1 ml/min. The organic portion was ramped from 5 to 25% B in 45 min to 40% in 10 min and finally to 70% in 5 min, followed by column equilibrated. Fractions were collected in 1-min intervals for 60 min and concatenated evenly into 30 pools. Acetonitrile was evaporated by vacuum centrifugation, and samples were acidified to pH 2 and measured by LC-MS/MS.

SDS–polyacrylamide gel electrophoresis and in-gel digestion

To obtain deeper coverage of the proteome sample, 50 μg of protein extract from one replicate of experiment 1 was separated via SDS–polyacrylamide gel electrophoresis (PAGE), and 10 gel slices were digested with either endoproteinase Lys-C [1:40 (w/w) in 20 mM ABC (ammonium bicarbonate)] or chymotrypsin [1:40 (w/w) in 50 mM tris (pH 8.0) and 10 mM $CaCl_2$], as described previously (*26*).

Incorporation and mixing check

The efficiency of SILAC labeling was determined by LC-MS/MS measurement of Lys4- and Lys8-labeled samples. For that, 10 μg of each sample was separately digested with endoproteinase Lys-C, purified by StageTips (see below), and measured by LC-MS/MS. In all cases, the labeling efficiencies of Lys4 or Lys8 were ≥94%. Before the mixing of labeled samples for SILAC experiments, 20 μg of each differentially labeled sample was premixed in equal protein amounts determined by Bradford assay, digested with endoproteinase Lys-C, and measured by LC-MS/MS. Median of evidence SILAC ratios was used as a correction factor for mixing the samples to be used in main SILAC experiments.

Protein purification by StageTips

Before each LC-MS/MS measurement, all peptide samples were desalted and purified on C18 StageTips (*53*). Reversed-phase C18 discs (Empore) were activated with methanol and equilibrated with solvent A*. Up to 10 μg of peptides was loaded onto the membrane and washed with solvent A. Peptides were eluted with 50 μl of solvent B [80% (v/v) acetonitrile and 0.1% (v/v) formic acid] and concentrated by vacuum centrifugation. The sample volume was adjusted with solvent A and final 10% (v/v) of solvent A*.

LC-MS/MS measurement

Purified peptide samples were separated by an EASY-nLC 1000 or 1200 system (Thermo Fisher Scientific) coupled online to a Q Exactive HF mass spectrometer (Thermo Fisher Scientific) through a nano-electrospray ion source (Thermo Fisher Scientific). Chromatographic separation was performed on a 20-cm-long, 75–μm–inner diameter analytical column packed in-house with reversed-phase ReproSil-Pur C18-AQ 1.9 μm particles (Dr. Maisch GmbH). The column temperature was maintained at 40°C using an integrated column oven. Peptides were loaded onto the column at a flow rate of 700 nl/min or 1 μl/min under maximum back pressure of 500 or 850 bar, respectively. The peptides were eluted using either 46-, 76-, 116-, or 216-min segmented gradient of 10 to 50% solvent B at a constant flow rate of 200 nl/min. When measuring proteome digested with chymotrypsin, the gradient started with 5% of solvent B. For measurements of kinase assays, the peptides were eluted using 33-min segmented gradient of 10 to 50%

solvent B at a constant flow rate of 300 nl/min. For measurement of samples fractionated by high-pH chromatography on column, different 76-min segmented gradients optimized for each fraction were used.

Peptides were ionized by nanoelectrospray ionization at 2.3 kV and the capillary temperature of 275°C. The mass spectrometer was operated in a data-dependent mode, switching automatically between one full scan and subsequent MS/MS scans of either 12 (Top12 method) or 7 (Top7 method, phosphoproteome measurement) most abundant peaks selected with an isolation window of 1.4 *m/z* (mass/charge ratio). Full-scan MS spectra were acquired in a mass range from 300 to 1650 *m/z* at a target value of 3×10^6 charges with the maximum injection time of 25 ms and a resolution of 60,000 (defined at *m/z* 200). The higher-energy collisional dissociation MS/MS spectra were recorded with the maximum injection time of 45 or 220 ms (for phosphoproteome measurement) at a target value of 1×10^5 and a resolution of 30,000 (defined at *m/z* 200) or 60,000 for phosphoproteome measurement. The normalized collision energy was set to 27%, and the intensity threshold was kept at 1×10^5 or 5×10^4 for phosphoproteome measurement. The masses of sequenced precursor ions were dynamically excluded from MS/MS fragmentation for 30 s. Ions with single, unassigned, or six and higher charge states were excluded from fragmentation selection. Two phosphoproteome experiments (chromosomal *hipA7*, experiments 1 and 3) were measured on an Orbitrap Elite mass spectrometer (Thermo Fisher Scientific) with previously described parameters (*54*).

MS data processing and analysis

Acquired raw data were processed using the MaxQuant software suite (version 1.5.2.8) (*55*). Raw files of particular experiments were processed separately (table S3). In total, we used 449 raw files, of which 249 belong to phosphopeptide enrichment fractions. The derived peak list was searched using Andromeda search engine integrated in MaxQuant (*56*) against a reference *E. coli* K-12 proteome (taxonomy ID 83333) obtained from UniProt (4313 protein entries, released in October 2015), protein sequence of HipA7, HipA mutants, and a file containing 245 common laboratory contaminants. During the first search, peptide mass tolerance was set to 20 ppm (parts per million) and, in the main search, to 4.5 ppm. For triple-label SILAC experiments, multiplicity was set to three with Lys4 and Lys8 specified as medium and heavy labels, respectively. Methionine oxidation, protein N-terminal acetylation, and Ser-Thr-Tyr phosphorylation were defined as variable modifications, and carbamidomethylation of cysteines was set as a fixed modification.

The minimum required peptide length was set to seven amino acids with the maximum of two missed cleavages allowed for endoproteinase Lys-C that was set to specifically cleave at lysine C terminus. Chymotrypsin was set to specifically cleave at phenylalanine, tryptophan, tyrosine, leucine, and methionine C terminus with maximum five missed cleavages allowing for maximum of four labeled amino acids. All (phospho)peptide and protein identifications were filtered using a target-decoy approach with a false discovery rate (FDR) set to 0.01 at peptide and protein level (*57*). Proteins identified by the same set of peptides were combined to a single protein group. Protein groups identified by a single peptide were kept in the data set. For protein quantification, a minimum of two peptide ratio counts was required. To increase the number of quantified features, the "match between runs" option was enabled with a match time window set to 0.7 min. This allows the transfer of peptide identifications across LC-MS/MS runs based on the mass and the retention time of the peptide identified by MS/MS. Requantify option was enabled to allow for quantification of SILAC pairs that result in extreme ratio values.

Statistical analysis of MaxQuant output data was performed manually or by using Perseus software (version 1.5.6.0) (*58*), and figures were edited in Adobe Illustrator. All contaminants and reverse hits were removed. Phosphorylation sites were additionally filtered for posterior error probability scores of <0.01. Minimal score of 40 was required for phosphorylation site and 20 for protein identifications. Changes in phosphorylation events were normalized to differences in protein abundances, unless otherwise stated. For that, phosphorylation site SILAC ratios were divided with the protein SILAC ratios of corresponding proteins. Normalized phosphorylation site ratios were $\log_2$-transformed and plotted against the $\log_{10}$-transformed phosphopeptide intensities summed for each of two SILAC channels observed. Statistically significantly regulated phosphorylation sites were determined by applying an arbitrary ratio threshold of 2 in $\log_2$ scale (fourfold). In the experiment with *hipA7* on the chromosome in which no plasmids were used, statistically significantly regulated phosphorylation sites were determined by using significance *B* test with a *P* value of 0.01. Statistically significantly regulated proteins were determined by using significance *B* test with a *P* value of 0.001. For Volcano plots, $\log_2$-transformed ratios of three independent experiments were grouped into one group and compared to the group containing only zero values using *t* test with FDR of 0.01 or 0.001 and the minimal fold change S0 of 1. Phosphorylation site occupancies were determined as the proportion between the phosphorylated peptide and corresponding unmodified peptide using the algorithm implemented in MaxQuant based on the calculation described by Olsen *et al.* (*32*). The calculation of occupancies requires SILAC ratio of a phosphorylated peptide, the SILAC ratio of the corresponding unmodified peptide, and the SILAC protein ratio. For RplK and SeqA, occupancy values were calculated manually using *M*/*L* and *H*/*M* ratios, giving *a* and *b* values between 0 and 1 in three independent experiments. For SeqA in "light" and RplK in "heavy" labeling state, occupancy was determined only from two independent experiments.

To identify significantly represented temporal protein profiles, we used Short Time-series Expression Miner (STEM) program (*P* value of 0.05 after Bonferroni multiple testing correction) (*59*). Gene annotation and Kyoto Encyclopedia of Genes and Genomes (KEGG) enrichment analysis was performed using the Database for Annotation, Visualization, and Integrated Discovery (DAVID) tool (version 6.7) with default parameters (*60*). UniProt IDs were used as an input for the enrichment. Kinase motif analysis was performed using motif-x software (*61*) with the reference *E. coli* proteome used as a background and 15–amino acid–slong sequences (seven amino acids on both sides around phosphorylation site) of all identified phosphorylation sites with the localization probability higher than 0.75 as an input. The parameters of motif-x analysis were as follows: S or T as a foreground and background central residue, width of 15, 40 occurrences, and significance threshold of 0.00000001.

Protein production for His-tag affinity purification

His_6-HipA and His_6-HipA7. Plasmid pBAD33::*6his hipA* was transformed into MG1655 strain. An overnight culture was grown in LB medium containing chloramphenicol (25 μg/ml) and 0.4% glucose, washed, diluted 1000× into 2 liters of LB medium containing chloramphenicol (25 μg/ml), and grown at 37°C. The expression of *hipA* and *hipA7* was induced at OD_{600nm} of 0.4 with 0.2% arabinose for 2 hours. His_6-HipA7 was produced from pBAD33::*6his hipA7* in 1 liter of LB medium in the same way as His_6-HipA.

His_6-GltX, His_6-RplK, and SeqA-His_6. Plasmid pET28a::*gltX* was transformed into BL21(DE3) strain. An overnight culture was grown in LB medium containing kanamycin (50 μg/ml), diluted 1000× into 250 ml of LB medium with kanamycin, and grown at 30°C. The expression of *gltX* was induced at OD_{600nm} of 0.6 with 1 mM IPTG for 2 hours. His_6-RplK was produced from the pET28a::*rplK* plasmid the same way as His_6-GltX. SeqA-His_6 was produced from the pET28a::*seqA* plasmid in 750 ml of LB medium the same way as His_6-GltX. The expression of *seqA* was induced at OD_{600nm} of 0.5 with 0.2 mM IPTG for 2 hours.

His-tag affinity purification

After the protein expression, cultures were harvested by centrifugation and cell pellets were resuspended in cold lysis buffer [50 mM Hepes/KOH (pH 7.4) at 4°C, 300 mM NaCl, 10 mM $MgCl_2$, 2 mM β-mercaptoethanol, EDTA-free protease inhibitors (Roche), 5 mM glycerol-2-phosphate, 5 mM sodium fluoride, and 1 mM sodium orthovanadate]. Each cell lysate was incubated with lysozyme (0.5 mg/ml) and deoxyribonuclease I (50 U/ml) for 15 min at RT, sonicated at 40% amplitude until clear, and centrifuged at 13,000*g*. Supernatant containing 10 mM imidazole was incubated with 500 μl of HisPur cobalt resin (Thermo Fisher Scientific) for 1 hour at 4°C. The cobalt resin was washed in buffer A [50 mM Hepes/KOH (pH 7.4) at 4°C, 300 mM NaCl, 10 mM $MgCl_2$, and 2 mM β-mercaptoethanol] containing 10, 20, or 30 mM imidazole. Bound proteins were eluted with buffer A containing 150 mM imidazole. Purified proteins were transferred into a storage buffer and concentrated by ultrafiltration using Amicon Ultra centrifugal filter units (Merck) with a pore size of 30,000 Da (for His_6-HipA, His_6-HipA7, and His_6-GltX) or 10,000 Da (for His_6-RplK and SeqA-His_6). Proteins were washed with storage buffer [50 mM tris-HCl (pH 8.0), 200 mM NaCl, and 1 mM DTT] and transferred into the storage buffer containing 10% glycerol. Protein concentration was measured using standard Bradford assay (Bio-Rad).

In vitro kinase assay measured by MS

Kinase (1 μM) (His_6-HipA or His_6-HipA7) was incubated with 6 μM His-tagged substrate in a kinase buffer [50 mM tris-HCl (pH 8.0), 10 mM $MgCl_2$, 1 mM DTT, and 16 μM $ZnSO_4$] with or without 5 mM ATP. Each reaction contained 4.5 μg of a total protein amount. Samples were incubated at 37°C for 45 min and stopped by the addition of nine volumes of denaturation buffer, followed by the protein digestion using chymotrypsin or Lys-C endoproteinase, as previously described (see above). Digested peptides were purified using StageTips (see above), and 0.2 μg of each sample was measured by LC-MS/MS (see above).

Dynamics of HipA and HipA7 in vitro (auto)phosphorylation measured by autoradiography

For qualitative comparison of HipA and HipA7 autophosphorylation activity and the phosphorylation activity toward GltX, we performed a time-depended kinase assay. Kinase (1 μM) (His_6-HipA or His_6-HipA7) was incubated with 54 μM ATP and 12 μM [γ-^{32}P]ATP and with or without 6 μM His_6-GltX and 19 μM of total *E. coli* tRNA in the kinase buffer [50 mM tris-HCl (pH 8.0), 10 mM $MgCl_2$, 1 mM DTT, and 16 μM $ZnSO_4$]. Reactions with HipA and HipA7 were performed simultaneously using the same ATP stock solution. The reactions were incubated at 37°C for 45 min and stopped by the addition of Laemmli buffer at indicated time points. Reaction mixtures were separated by SDS-PAGE, revealed by phosphorimaging (GE Healthcare), and analyzed using ImageQuant software (GE Healthcare). The intensity of each time point was normalized to the sum of intensities of all time points and presented as a fraction of total intensity. Phosphorylation activity was determined by the linear regression of the linear part of the intensity over time curve.

Determination of cell viability on SMG plates

It is known that Δ*relA* mutant exhibits relaxed phenotype when grown in the presence of single carbon amino acids (SMG) (*31*). *E. coli* MG1555, *rplK* S102A, *rplK* S102D, and Δ*relA* deletion mutant (table S1) were grown in M9 medium with glucose for 24 hours to stationary phase. Aliquots of cells were serially diluted in M9 medium, plated on M9 agar plates supplemented with or without 1 mM amino acids SMG, and grown for 40 hours at 37°C.

Measurement of persistence

Cells were grown in 20 ml of M9 medium with glycerol containing chloramphenicol (25 μg/ml) and ampicillin (25 μg/ml) to the exponential phase. At OD_{600nm} of around 0.4, *hipA* was induced with 0.2% arabinose for 95 min. Cultures were then treated with ciprofloxacin (2 μg/ml; Sigma-Aldrich) for 5 hours. For determination of colony-forming units (CFU), 1 ml of aliquots was taken before arabinose addition, 95 min after *hipA* induction, and 5 hours of ciprofloxacin treatment. Cells were washed with phosphate-buffered saline, serially diluted, plated on LB agar plates containing 0.4% glucose, and grown for 24 to 40 hours at 37°C. Persistence was calculated by dividing the number of CFU/ml of ciprofloxacin-treated culture with the CFU/ml of the culture before antibiotic addition and presented as a frequency of surviving (persister) cells in log_{10} scale.

SUPPLEMENTARY MATERIALS

www.sciencesignaling.org/cgi/content/full/11/547/eaat5750/DC1

Fig. S1. Additional analysis of phosphoproteomic data from HipA-induced growth inhibition and HipB-induced resuscitation and follow-up experiments.

Fig. S2. Additional analysis of phosphoproteomic data from comparably overproduced HipA and HipA7.

Fig. S3. Additional analysis of phosphoproteomic data from low and high production of HipA and HipA7.

Fig. S4. Additional analysis of phosphoproteomic data from *hipA7* and *wt hipA* strains.

Fig. S5. Functional analysis of the *E. coli* phosphoproteome obtained in this study.

Table S1. Bacterial strains and plasmids.

Table S2. DNA oligonucleotides.

Table S3. Overview of all experiments measured by LC-MS/MS.

Data file S1. Protein groups and phosphorylation sites identified in this study.

REFERENCES AND NOTES

1. N. Q. Balaban, Persistence: Mechanisms for triggering and enhancing phenotypic variability. *Curr. Opin. Genet. Dev.* **21**, 768–775 (2011).
2. N. Q. Balaban, J. Merrin, R. Chait, L. Kowalik, S. Leibler, Bacterial persistence as a phenotypic switch. *Science* **305**, 1622–1625 (2004).
3. K. Lewis, Persister cells. *Annu. Rev. Microbiol.* **64**, 357–372 (2010).
4. K. Lewis, Persister cells, dormancy and infectious disease. *Nat. Rev. Microbiol.* **5**, 48–56 (2006).
5. M. A. Schumacher, P. Balani, J. Min, N. B. Chinnam, S. Hansen, M. Vulić, K. Lewis, R. G. Brennan, HipBA–promoter structures reveal the basis of heritable multidrug tolerance. *Nature* **524**, 59–64 (2015).
6. L. R. Mulcahy, J. L. Burns, S. Lory, K. Lewis, Emergence of *Pseudomonas aeruginosa* strains producing high levels of persister cells in patients with cystic fibrosis. *J. Bacteriol.* **192**, 6191–6199 (2010).
7. B. Van den Bergh, M. Fauvart, J. Michiels, Formation, physiology, ecology, evolution and clinical importance of bacterial persisters. *FEMS Microbiol. Rev.* **41**, 219–251 (2017).
8. I. Keren, N. Kaldalu, A. Spoering, Y. Wang, K. Lewis, Persister cells and tolerance to antimicrobials. *FEMS Microbiol. Lett.* **230**, 13–18 (2004).
9. A. Harms, E. Maisonneuve, K. Gerdes, Mechanisms of bacterial persistence during stress and antibiotic exposure. *Science* **354**, aaf4268 (2016).

10. A. Harms, D. E. Brodersen, N. Mitarai, K. Gerdes, Toxins, targets, and triggers: An overview of toxin-antitoxin biology. *Mol. Cell* **70**, 768–784 (2018).
11. H. S. Moyed, K. P. Bertrand, hipA, a newly recognized gene of *Escherichia coli* K-12 that affects frequency of persistence after inhibition of murein synthesis. *J. Bacteriol.* **155**, 768–775 (1983).
12. S. B. Korch, T. A. Henderson, T. M. Hill, Characterization of the *hipA7* allele of *Escherichia coli* and evidence that high persistence is governed by (p)ppGpp synthesis. *Mol. Microbiol.* **50**, 1199–1213 (2003).
13. S. B. Korch, T. M. Hill, Ectopic overexpression of wild-type and mutant *hipA* genes in *Escherichia coli*: Effects on macromolecular synthesis and persister formation. *J. Bacteriol.* **188**, 3826–3836 (2006).
14. D. S. Black, B. Irwin, H. S. Moyed, Autoregulation of hip, an operon that affects lethality due to inhibition of peptidoglycan or DNA synthesis. *J. Bacteriol.* **176**, 4081–4091 (1994).
15. E. Germain, D. Castro-Roa, N. Zenkin, K. Gerdes, Molecular mechanism of bacterial persistence by HipA. *Mol. Cell* **52**, 248–254 (2013).
16. I. Kaspy, E. Rotem, N. Weiss, I. Ronin, N. Q. Balaban, G. Glaser, HipA-mediated antibiotic persistence via phosphorylation of the glutamyl-tRNA-synthetase. *Nat. Commun.* **4**, 3001 (2013).
17. G. Bokinsky, E. E. K. Baidoo, S. Akella, H. Burd, D. Weaver, J. Alonso-Gutierrez, H. García-Martín, T. S. Lee, J. D. Keasling, HipA-triggered growth arrest and β-lactam tolerance in *Escherichia coli* are mediated by RelA-dependent ppGpp synthesis. *J. Bacteriol.* **195**, 3173–3182 (2013).
18. A. B. Loveland, E. Bah, R. Madireddy, Y. Zhang, A. F. Brilot, N. Grigorieff, A. A. Korostelev, Ribosome•RelA structures reveal the mechanism of stringent response activation. *eLife* **5**, e17029 (2016).
19. T. M. Wendrich, G. Blaha, D. N. Wilson, M. A. Marahiel, K. H. Nierhaus, Dissection of the mechanism for the stringent factor RelA. *Mol. Cell* **10**, 779–788 (2002).
20. X. Yang, E. E. Ishiguro, Involvement of the N terminus of ribosomal protein L11 in regulation of the RelA protein of *Escherichia coli*. *J. Bacteriol.* **183**, 6532–6537 (2001).
21. E. Rotem, A. Loinger, I. Ronin, I. Levin-Reisman, C. Gabay, N. Shoresh, O. Biham, N. Q. Balaban, Regulation of phenotypic variability by a threshold-based mechanism underlies bacterial persistence. *Proc. Natl. Acad. Sci. U.S.A.* **107**, 12541–12546 (2010).
22. A. Kalantari, A. Derouiche, L. Shi, I. Mijakovic, Serine/threonine/tyrosine phosphorylation regulates DNA binding of bacterial transcriptional regulators. *Microbiology* **161**, 1720–1729 (2015).
23. L. Shi, N. Pigeonneau, V. Ravikumar, P. Dobrinic, B. Macek, D. Franjevic, M.-F. Noirot-Gros, I. Mijakovic, Cross-phosphorylation of bacterial serine/threonine and tyrosine protein kinases on key regulatory residues. *Front. Microbiol.* **5**, 495 (2014).
24. M. A. Schumacher, K. M. Piro, W. Xu, S. Hansen, K. Lewis, R. G. Brennan, Molecular mechanisms of HipA-mediated multidrug tolerance and its neutralization by HipB. *Science* **323**, 396–401 (2009).
25. S.-E. Ong, B. Blagoev, I. Kratchmarova, D. B. Kristensen, H. Steen, A. Pandey, M. Mann, Stable isotope labeling by amino acids in cell culture, SILAC, as a simple and accurate approach to expression proteomics. *Mol. Cell. Proteomics* **1**, 376–386 (2002).
26. V. Ravikumar, L. Shi, K. Krug, A. Derouiche, C. Jers, C. Cousin, A. Kobir, I. Mijakovic, B. Macek, Quantitative phosphoproteome analysis of *Bacillus subtilis* reveals novel substrates of the kinase PrkC and phosphatase PrpC. *Mol. Cell. Proteomics* **13**, 1965–1978 (2014).
27. D. S. Black, A. J. Kelly, M. J. Mardis, H. S. Moyed, Structure and organization of hip, an operon that affects lethality due to inhibition of peptidoglycan or DNA synthesis. *J. Bacteriol.* **173**, 5732–5739 (1991).
28. F. F. Correia, A. D'Onofrio, T. Rejtar, L. Li, B. L. Karger, K. Makarova, E. V. Koonin, K. Lewis, Kinase activity of overexpressed HipA is required for growth arrest and multidrug tolerance in *Escherichia coli*. *J. Bacteriol.* **188**, 8360–8367 (2006).
29. M. A. Schumacher, J. Min, T. M. Link, Z. Guan, W. Xu, Y.-H. Ahn, E. J. Soderblom, J. M. Kurie, A. Evdokimov, M. A. Moseley, K. Lewis, R. G. Brennan, Role of unusual P-loop ejection and autophosphorylation in HipA-mediated persistence and multidrug tolerance. *Cell Rep.* **2**, 518–525 (2012).
30. V. Hauryliuk, G. C. Atkinson, K. S. Murakami, T. Tenson, K. Gerdes, Recent functional insights into the role of (p)ppGpp in bacterial physiology. *Nat. Rev. Microbiol.* **13**, 298–309 (2015).
31. M. Uzan, A. Danchin, A rapid test for the rel A mutation in *E. coli*. *Biochem. Biophys. Res. Commun.* **69**, 751–758 (1976).
32. J. V. Olsen, M. Vermeulen, A. Santamaria, C. Kumar, M. L. Miller, L. J. Jensen, F. Gnad, J. Cox, T. S. Jensen, E. A. Nigg, S. Brunak, M. Mann, Quantitative phosphoproteomics reveals widespread full phosphorylation site occupancy during mitosis. *Sci. Signal.* **3**, ra3 (2010).
33. P. Klemm, L. Hjerrild, M. Gjermansen, M. A. Schembri, Structure-function analysis of the self-recognizing antigen 43 autotransporter protein from *Escherichia coli*. *Mol. Microbiol.* **51**, 283–296 (2004).
34. J. L. Brissette, L. Weiner, T. L. Ripmaster, P. Model, Characterization and sequence of the *Escherichia coli* stress-induced *psp* operon. *J. Mol. Biol.* **220**, 35–48 (1991).
35. Y. Pu, Z. Zhao, Y. Li, J. Zou, Q. Ma, Y. Zhao, Y. Ke, Y. Zhu, H. Chen, M. A. B. Baker, H. Ge, Y. Sun, X. S. Xie, F. Bai, Enhanced efflux activity facilitates drug tolerance in dormant bacterial cells. *Mol. Cell* **62**, 284–294 (2016).
36. I. Keren, D. Shah, A. Spoering, N. Kaldalu, K. Lewis, Specialized persister cells and the mechanism of multidrug tolerance in *Escherichia coli*. *J. Bacteriol.* **186**, 8172–8180 (2004).
37. D. Shah, Z. Zhang, A. B. Khodursky, N. Kaldalu, K. Kurg, K. Lewis, Persisters: A distinct physiological state of *E. coli*. *BMC Microbiol.* **6**, 53 (2006).
38. F. von Delft, A. Lewendon, V. Dhanaraj, T. L. Blundell, C. Abell, A. G. Smith, The crystal structure of *E. coli* pantothenate synthetase confirms it as a member of the cytidylyltransferase superfamily. *Structure* **9**, 439–450 (2001).
39. M.-H. Lin, N. Sugiyama, Y. Ishihama, Systematic profiling of the bacterial phosphoproteome reveals bacterium-specific features of phosphorylation. *Sci. Signal.* **8**, rs10 (2015).
40. C. M. Potel, M.-H. Lin, A. J. R. Heck, S. Lemeer, Widespread bacterial protein histidine phosphorylation revealed by mass spectrometry-based proteomics. *Nat. Methods* **15**, 187–190 (2018).
41. E. Maisonneuve, K. Gerdes, Molecular mechanisms underlying bacterial persisters. *Cell* **157**, 539–548 (2014).
42. M. Lu, J. L. Campbell, E. Boye, N. Kleckner, SeqA: A negative modulator of replication initiation in *E. coli*. *Cell* **77**, 413–426 (1994).
43. X.-P. Guo, Y.-C. Sun, New insights into the non-orthodox two component Rcs phosphorelay system. *Front. Microbiol.* **8**, 2014 (2017).
44. M. Wehland, F. Bernhard, The RcsAB box: Characterization of a new operator essential for the regulation of exopolysaccharide biosynthesis in enteric bacteria. *J. Biol. Chem.* **275**, 7013–7020 (2000).
45. L. Hoang, K. Fredrick, H. F. Noller, Creating ribosomes with an all-RNA 30S subunit P site. *Proc. Natl. Acad. Sci. U.S.A.* **101**, 12439–12443 (2004).
46. R. K. Agrawal, J. Linde, J. Sengupta, K. H. Nierhaus, J. Frank, Localization of L11 protein on the ribosome and elucidation of its involvement in EF-G-dependent translocation. *J. Mol. Biol.* **311**, 777–787 (2001).
47. Y. Maeda, C.-Y. Lin, Y. Ishida, M. Inouye, Y. Yamaguchi, S. Phadtare, Characterization of YjjJ toxin of *Escherichia coli*. *FEMS Microbiol. Lett.* **364**, fnx086 (2017).
48. G. C. Ulett, J. Valle, C. Beloin, O. Sherlock, J.-M. Ghigo, M. A. Schembri, Functional analysis of antigen 43 in uropathogenic *Escherichia coli* reveals a role in long-term persistence in the urinary tract. *Infect. Immun.* **75**, 3233–3244 (2007).
49. S. Ringquist, S. Shinedling, D. Barrick, L. Green, J. Binkley, G. D. Stormo, L. Gold, Translation initiation in *Escherichia coli*: Sequences within the ribosome-binding site. *Mol. Microbiol.* **6**, 1219–1229 (1992).
50. A. J. Link, D. Phillips, G. M. Church, Methods for generating precise deletions and insertions in the genome of wild-type *Escherichia coli*: Application to open reading frame characterization. *J. Bacteriol.* **179**, 6228–6237 (1997).
51. T. Tabone, D. E. Mather, M. J. Hayden, Temperature switch PCR (TSP): Robust assay design for reliable amplification and genotyping of SNPs. *BMC Genomics* **10**, 580 (2009).
52. B. Soufi, B. Macek, Stable isotope labeling by amino acids applied to bacterial cell culture. *Methods Mol. Biol.* **1188**, 9–22 (2014).
53. J. Rappsilber, M. Mann, Y. Ishihama, Protocol for micro-purification, enrichment, pre-fractionation and storage of peptides for proteomics using StageTips. *Nat. Protoc.* **2**, 1896–1906 (2007).
54. N. Cvetesic, M. Semanjski, B. Soufi, K. Krug, I. Gruic-Sovulj, B. Macek, Proteome-wide measurement of non-canonical bacterial mistranslation by quantitative mass spectrometry of protein modifications. *Sci. Rep.* **6**, 28631 (2016).
55. J. Cox, M. Mann, MaxQuant enables high peptide identification rates, individualized p.p.b.-range mass accuracies and proteome-wide protein quantification. *Nat. Biotechnol.* **26**, 1367–1372 (2008).
56. J. Cox, N. Neuhauser, A. Michalski, R. A. Scheltema, J. V. Olsen, M. Mann, Andromeda: A peptide search engine integrated into the MaxQuant environment. *J. Proteome Res.* **10**, 1794–1805 (2011).
57. J. E. Elias, S. P. Gygi, Target-decoy search strategy for increased confidence in large-scale protein identifications by mass spectrometry. *Nat. Methods* **4**, 207–214 (2007).
58. S. Tyanova, T. Temu, P. Sinitcyn, A. Carlson, M. Y. Hein, T. Geiger, M. Mann, J. Cox, The Perseus computational platform for comprehensive analysis of (prote)omics data. *Nat. Methods* **13**, 731–740 (2016).
59. J. Ernst, Z. Bar-Joseph, STEM: A tool for the analysis of short time series gene expression data. *BMC Bioinformatics* **7**, 191 (2006).
60. D. W. Huang, B. T. Sherman, R. A. Lempicki, Systematic and integrative analysis of large gene lists using DAVID bioinformatics resources. *Nat. Protoc.* **4**, 44–57 (2009).
61. D. Schwartz, S. P. Gygi, An iterative statistical approach to the identification of protein phosphorylation motifs from large-scale data sets. *Nat. Biotechnol.* **23**, 1391–1398 (2005).

62. J. A. Vizcaíno, A. Csordas, N. del-Toro, J. A. Dianes, J. Griss, I. Lavidas, G. Mayer, Y. Perez-Riverol, F. Reisinger, T. Ternent, Q.-W. Xu, R. Wang, H. Hermjakob, 2016 update of the PRIDE database and its related tools. *Nucleic Acids Res.* **44**, D447–D456 (2016).

Acknowledgments: We thank J. Schwickert and S. V. Nielsen for help with the experiments. M.S. is an external member of the Graduate College GRK1708 "Molecular principles of bacterial survival strategies." **Funding:** This work was supported by a grant from the Danish National Research Foundation to K.G. (grant identifier DNRF120), the Novo Nordisk Foundation (to K.G.), and the SFB 766 of the German Research Foundation (to B.M.). **Author contributions:** M.S., E.G., B.M., and K.G. designed the project. M.S. performed the experiments together with A.K. and K.B., whereas E.G. provided some of *E. coli* strains. M.S. analyzed the data. M.S. and B.M. wrote the manuscript with input from all authors. **Competing interests:** The authors declare that they have no competing financial interests. **Data and materials availability:** The MS data have been deposited to the ProteomeXchange Consortium (http://proteomecentral.proteomexchange.org/) through the PRIDE partner repository (*62*) with the data set identifier PXD009173. All other data needed to evaluate the conclusions in this paper are present in the paper or the Supplementary Materials.

Submitted 13 March 2018
Accepted 13 August 2018
Published 11 September 2018
10.1126/scisignal.aat5750

Citation: M. Semanjski, E. Germain, K. Bratl, A. Kiessling, K. Gerdes, B. Macek, The kinases HipA and HipA7 phosphorylate different substrate pools in *Escherichia coli* to promote multidrug tolerance. *Sci. Signal.* **11**, eaat5750 (2018).

Science Signaling

The kinases HipA and HipA7 phosphorylate different substrate pools in *Escherichia coli* to promote multidrug tolerance

Maja Semanjski, Elsa Germain, Katrin Bratl, Andreas Kiessling, Kenn Gerdes and Boris Macek

Sci. Signal. **11** (547), eaat5750.
DOI: 10.1126/scisignal.aat5750

Balancing bacterial growth with drug resistance

Within some bacterial populations, a subset of cells grows more slowly than the rest, which decreases the competitive fitness of these cells under favorable growth conditions but enables them to survive exposure to antibiotics. The kinase HipA is important for the survival of such *Escherichia coli* persister cells because it targets the glutamate-tRNA ligase GltX, thus halting translation and slowing cell growth. A variant of this kinase that is associated with some clinical isolates, HipA7, is more efficient than HipA in inducing persistence, although it is less effective at reducing cell growth. Through phosphoproteomic analyses, Semanjski *et al*. found that although both HipA and HipA7 targeted GltX, HipA also targeted additional substrates, which likely account for the potency of HipA in reducing cell growth and may explain why HipA7, despite being more effective at promoting persistence, is less toxic than HipA.